

Krzysztof Ostrowski

Institute of Heat Engineering
Warsaw University of Technology

MEASUREMENTS OF TWO-PHASE, DISPERSED FLOW PERTURBATIONS WITH SPECIAL REGARD TO HEAT TRANSFER PHENOMENA

The paper presents results of the heat flux fluctuations measurements performed on the surface of the horizontal cylinder 29 mm in diameter, mounted in vertical column, 0.19 m I.D. The air flow through a stagnant water was tested with its flow rates under the bubble, transition and churn flow regimes. In order to analyze the influence of liquid eddies of various scales approaching the cylinder surface the hot-film anemometer with 0.2×0.75 mm heated film was used in a constant temperature system. Statistical analysis of recorded signals was performed and some properties of the fluctuations are presented versus air superficial velocity, void fraction and sensor position. According to the obtained data the main intensification of the transport processes results from the random and local but anisotropic perturbations.

Nomenclature

<i>ACF</i>	– autocorrelation function
<i>E</i>	– sensor voltage (E_0 – for zero gas flow rate)
<i>H</i>	– height of air-water mixture (H_0 – water height for no gas flow)
<i>PSD</i>	– power spectral density function
R_{op}	– sensor operating resistance
$\overline{W} = E^2/E_0^2$	– nondimensional heat losses
\overline{W}	– mean value of <i>W</i>
V_G	– air superficial velocity (air flow rate/column cross section) in the inlet section
α	– averaged void fraction
φ	– sensor angle (see Fig. 2a,b)

An essential feature of gas-liquid flow is the existence of perturbations having various scales and frequencies. Contrary to a single-phase turbulent flow they appear not only due to the energy inertial transfer from the large scales, but also as the effect of the relative motion of both phases coupled with the interface deformation of exceedingly complex character. As the result of this, there is no clear distinction between the laminar and turbulent regimes of such a flow. In fact, the significant movement in the small scales can be encountered even for the astonishingly low gas and liquid flow rates.

The direct influence of this phenomenon on the mass, heat and momentum transport is a well known fact. For example, the numerous investigations (e.g. [1, 2]) of heat transfer from the wall and immersed elements of the vertical flow of gas-liquid mixture have clearly showed the heat transfer coefficients are many times larger than for single-phase flow. The obtained values exceeded $5000 \text{ W}/(\text{m}^2 \cdot \text{K})$ for the gas superficial velocity as low as 0.1 m/s and the zero liquid flow rate. However, the mechanism of the phenomenon has not been yet clearly understood. Kast [3] was the first who noticed that the usual concept of heat transfer through the boundary layer does not apply to the fluid motion caused by the relative movement of one phase with respect to the other. Various models were proposed to relate transport coefficients with the flow properties, the most widely used being the energy dissipation analysis based on the Kolmogoroff's isotropic turbulence model, e.g. [4, 5]. However, for some regimes of the two-phase, buoyancy driven, dispersed flows even the small eddies may be anisotropic, so the validity of this approach should be checked in more detail. In fact, the influence of particular bands of the perturbation frequencies on the transport phenomena remains unknown.

This paper presents results of the experiments directed towards identification of small-scale perturbations interactions on heat transfer in the immediate vicinity of the rigid surface in a vertical column under bubble, transition and churn flow regimes, defined [6, 7] as follows (Fig. 1):

- bubble flow: small gas bubbles are dispersed homogeneously in the liquid phase,
- transition regime: the dispersed flow is not homogeneous due to large and slow perturbations of void fraction – identified ([8, 9]) as clouds of small bubbles for which distinctive large slugs are not observable,
- churn flow: the bulk of the gas phase flows in the form of large bubbles having irregular shapes and dimensions comparable with the diameter of the column.

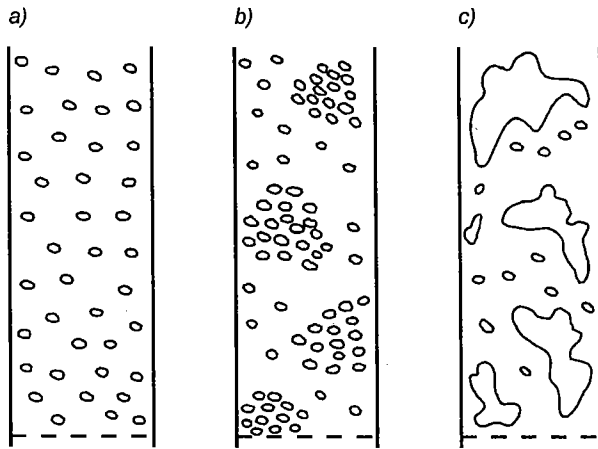


Fig. 1. Flow patterns (regimes) tested in the present experiment: a) bubble, b) transition, c) churn flow

It is necessary to distinguish between the bubble flow and the transition or churn flow regime. In the former the energy is supplied directly to the small (i.e. comparable with the diameter of small bubbles) scales, while the latter contains perturbations of the wide band of sizes and frequencies. Thus, the heat transfer for the particular flow regime is affected by the quite different interactions.

1. EXPERIMENTAL SET-UP AND DATA ACQUISITION

A schematic diagram of the experimental set-up is shown in Fig. 2a, b. In order to exclude the influence of the shear flow of the continuous phase, the air flow through stagnant water has been tested in a vertical column 2 m high, 0.19 m I.D., at atmospheric pressure and room temperature. The column (2) was constructed of transparent perspex, 5 mm thick, to facilitate the visual observations of the flow regime. To minimize the fluctuations of gas pressure, a gas chamber (6), 0.3 m high and of the same diameter as the column, was attached to the column bottom.

The dispersion of air as bubbles was achieved by passing the air through the sieve-plate (5) into the water. The sieve-plate, partitioning the column and the gas-chamber, was made from the copper plate, 0.3 mm thick, with 450 drilled holes, 0.5 mm in diameter. The typical equivalent radius of the generated bubbles was equal to 2–4 mm. The column was operated continuously.

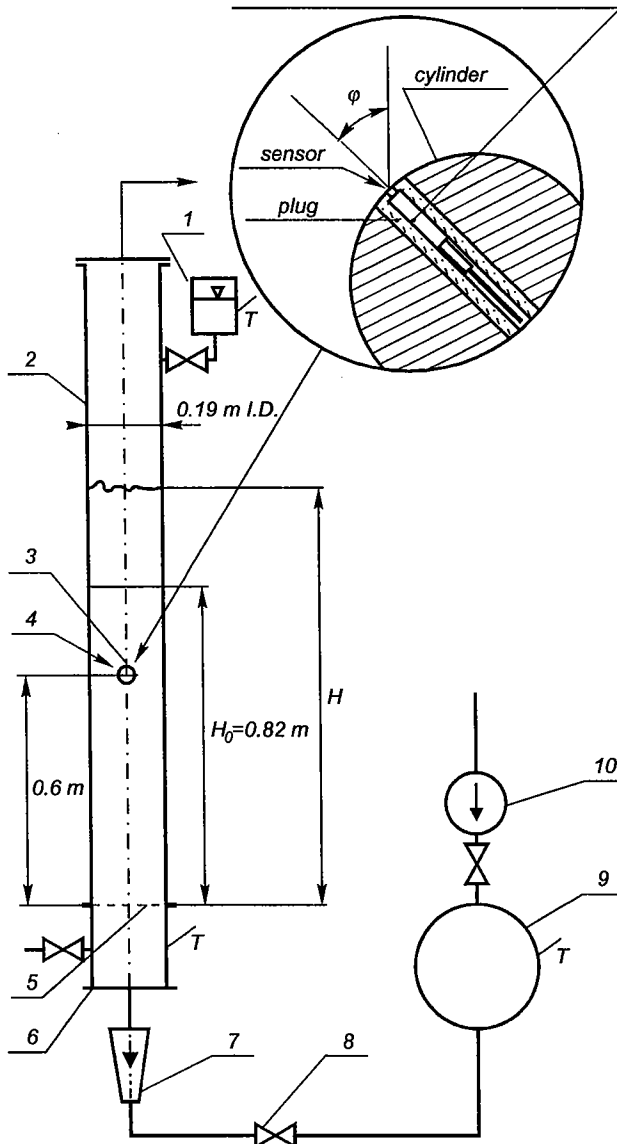


Fig. 2a. Experimental set-up: 1 – water storage tank, 2 – column, 3 – copper cylinder 29 mm in diameter, 4 – hot-film anemometer, 5 – sieve-plate, 6 – gas chamber, 7 – air rotameter, 8 – control valve, 9 – calming tank, 10 – rotary blower

Air supplied by the rotary blower (10) was fed into the gas chamber through the calming tank (9), control valve (8) and rotameter (7). A distilled water was charged into the column after its temperature was controlled in a storage tank (1). The air superficial velocity V_G ranged from zero up to 0.18 m/s,

b)

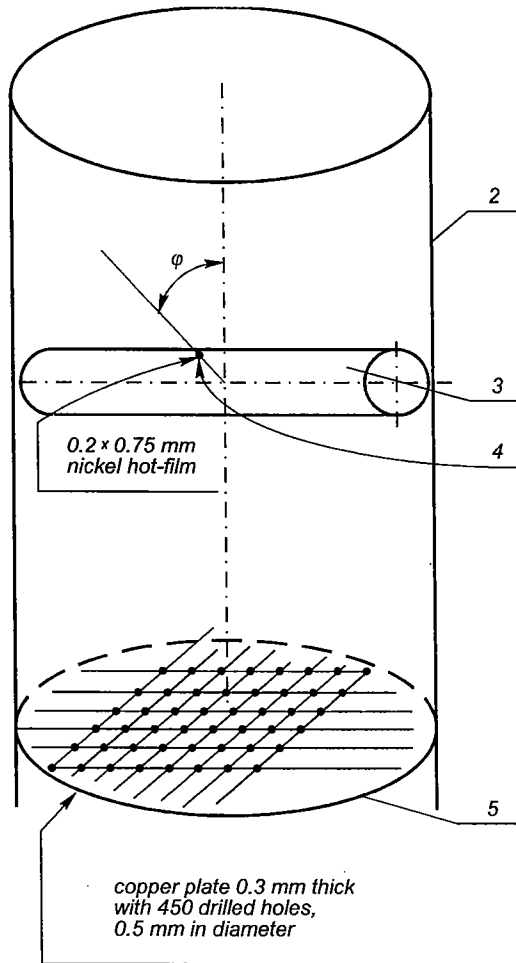


Fig. 2b. Experimental set-up: 2 – transparent column, 3 – copper cylinder, 4 – sensor of hot-film anemometer, 5 – sieve-plate (gas distributor)

which corresponds to the bubble, transition and churn flow regimes. The averaged void fraction in the column was obtained by measuring the level of the aerated water during operation H , and that of clear water H_0 ($H_0 = 0.82$ m for all measurements). Thus, the average void fraction α is given as:

$$\alpha = (H - H_0) / H$$

with a relative error varying from 5% for bubble regime up to 15% for churn regime ([9]).

In order to obtain information on the local and instant interactions between the liquid eddies and the rigid surface, the changes of heat flux on a small heated element has been measured by means of the hot-film anemometer.

55R46 DANTEC hot-film, flush-mounting probe was used in a constant temperature system. This probe has 0.2×0.75 mm nickel film deposited on a quartz cylindrical base and protected by a quartz film of about $2 \mu\text{m}$ thickness to secure the nickel sensor against breakthrough and against electrolysis. The probe was inserted in a perspex plug and then mounted in a hole in the cylinder (3), placed horizontally in the column 0.6 m above the sieve-plate, so that the sensor was positioned flush with its surface. The measurements were performed for the seven sensor positions, i.e. for angle $\varphi = 0^\circ, 30^\circ, 60^\circ, 90^\circ, 120^\circ, 150^\circ$ and 180° (Fig. 2a, b).

Temperature coefficient of sensor resistance at 20°C and sensor resistance at 20°C were $0.41\%/^\circ\text{C}$ and 8.25Ω , respectively. The overheat ratio was selected as 1.12, which corresponded to the temperature difference between the nickel sensor and the water in the column equal to 26°C and sensor operating resistance $R_{\text{op}} = 9.23 \Omega$. The output voltage signal from the bridge, corresponding to the sensor voltage – E was sampled and digitized with the 10-bit analog-to-digital converter and fed into IBM personal computer.

Sampling rate was selected as 500 Hz. This value exceeded many times the bubbles passage frequency which is no higher than 30 Hz. However, according to previous results [10, 11, 12], the signals contain impulses of large amplitude and typical pulse width close to 0.05 s. Thus, the sampling frequency was selected in order to analyze this phenomenon in more detail.

Each one of the recorded signals contained 4096 data points so the total record time was close to 8 s. The latter value corresponds to a period of large and slow void fraction perturbations typical for the transition regime [8].

2. RESULTS

Some of the recorded signals are presented in Fig. 3, 4, 5 in the form of non-dimensional sensor heat losses fluctuations: $W = E^2/E_0^2$. For the selected system conditions the E_0 values were equal to 0.60, 0.61 and 0.59 V for angle $\varphi = 0^\circ, 90^\circ$ and 180° respectively, with their standard deviation smaller than 1 mV. Thus, E_0^2/R_{op} is close to 0.04 W. The latter value is large, because of the significant heat conduction through the quartz base of the probe. It is necessary to point out that since the probe was not calibrated the instant values of W could not be related to the sensor surface.

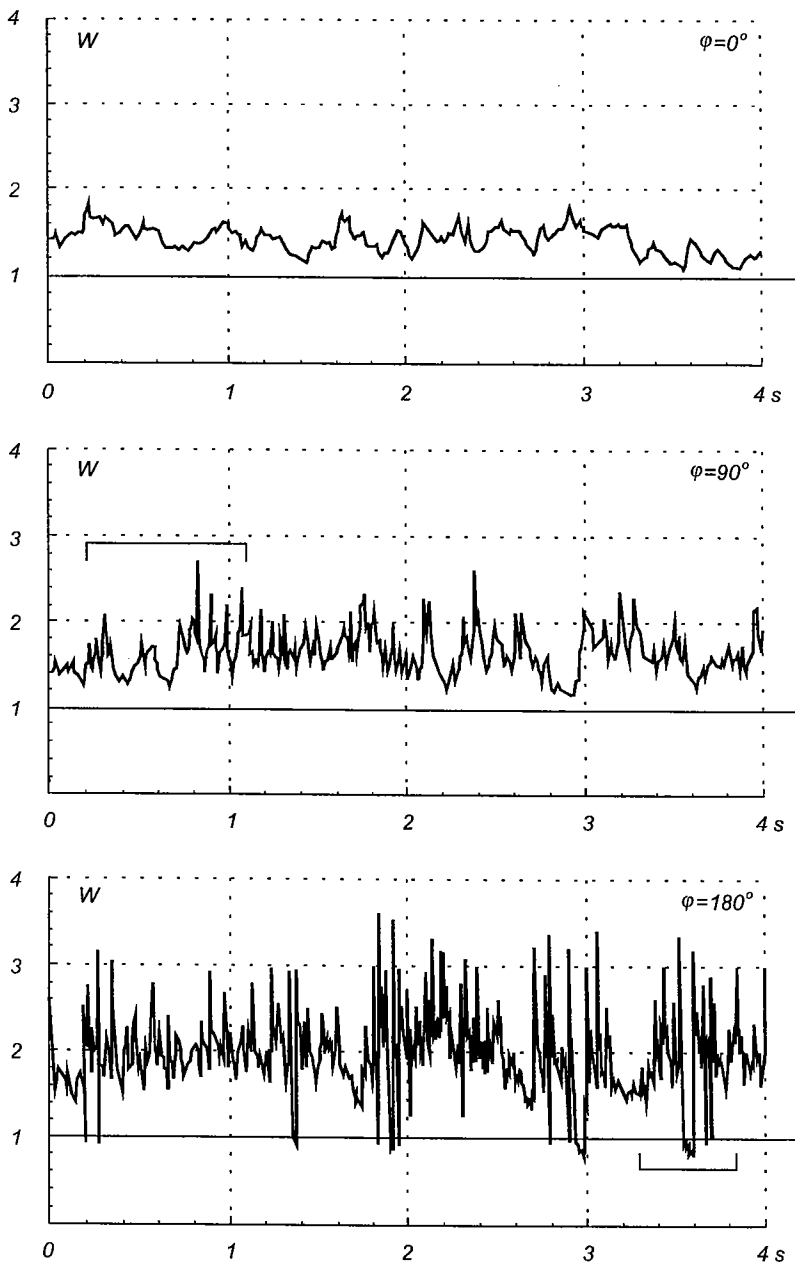


Fig. 3a. W fluctuations for $V_G = 0.021$ m/s, $\alpha = 0.10$, $\varphi = 0, 90$ and 180° , bubble regime

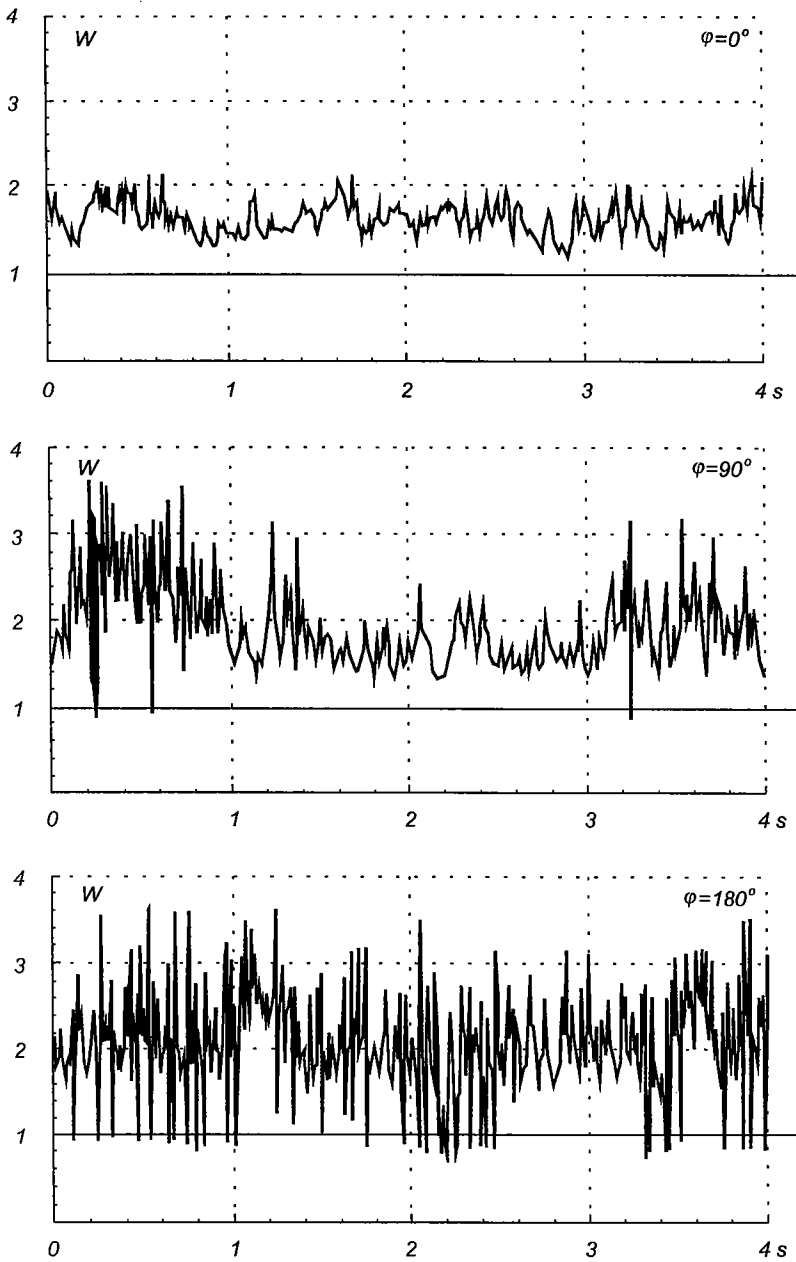


Fig. 3b. W fluctuations for $V_G = 0.063$ m/s, $\alpha = 0.10$, $\varphi = 0, 90$ and 180° , transition regime

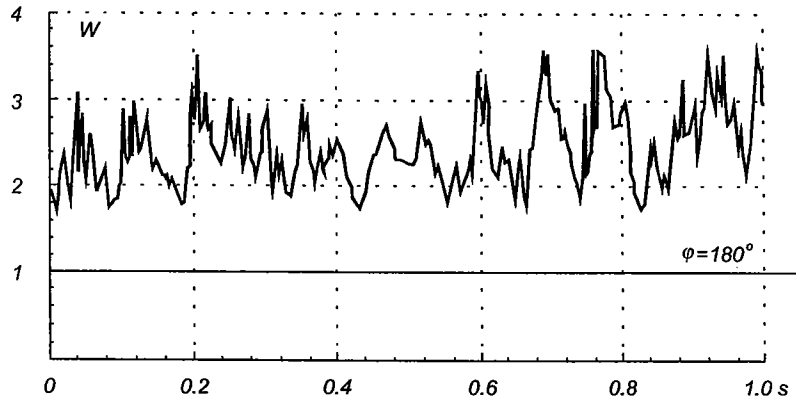
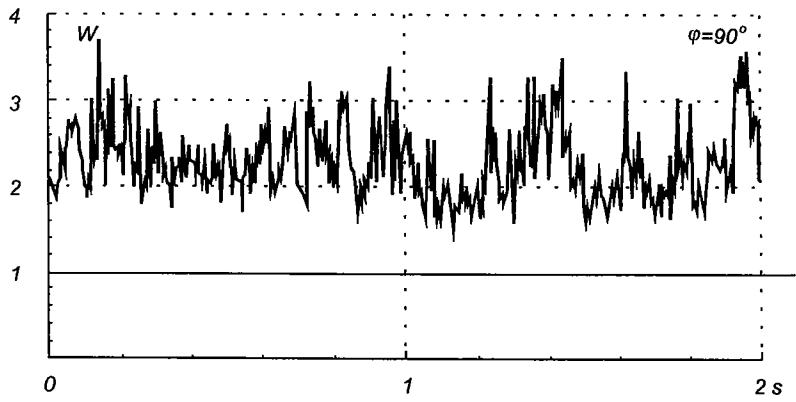
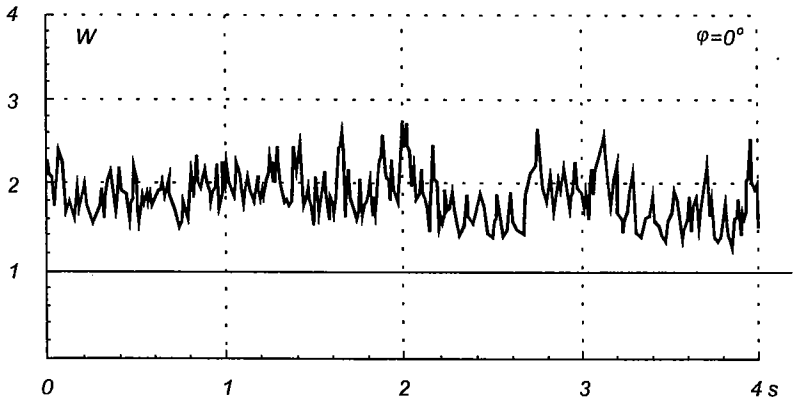


Fig. 3c. W fluctuations for $V_G = 0.158$ m/s, $\alpha = 0.10$, $\varphi = 0, 90$ and 180° , churn flow regime

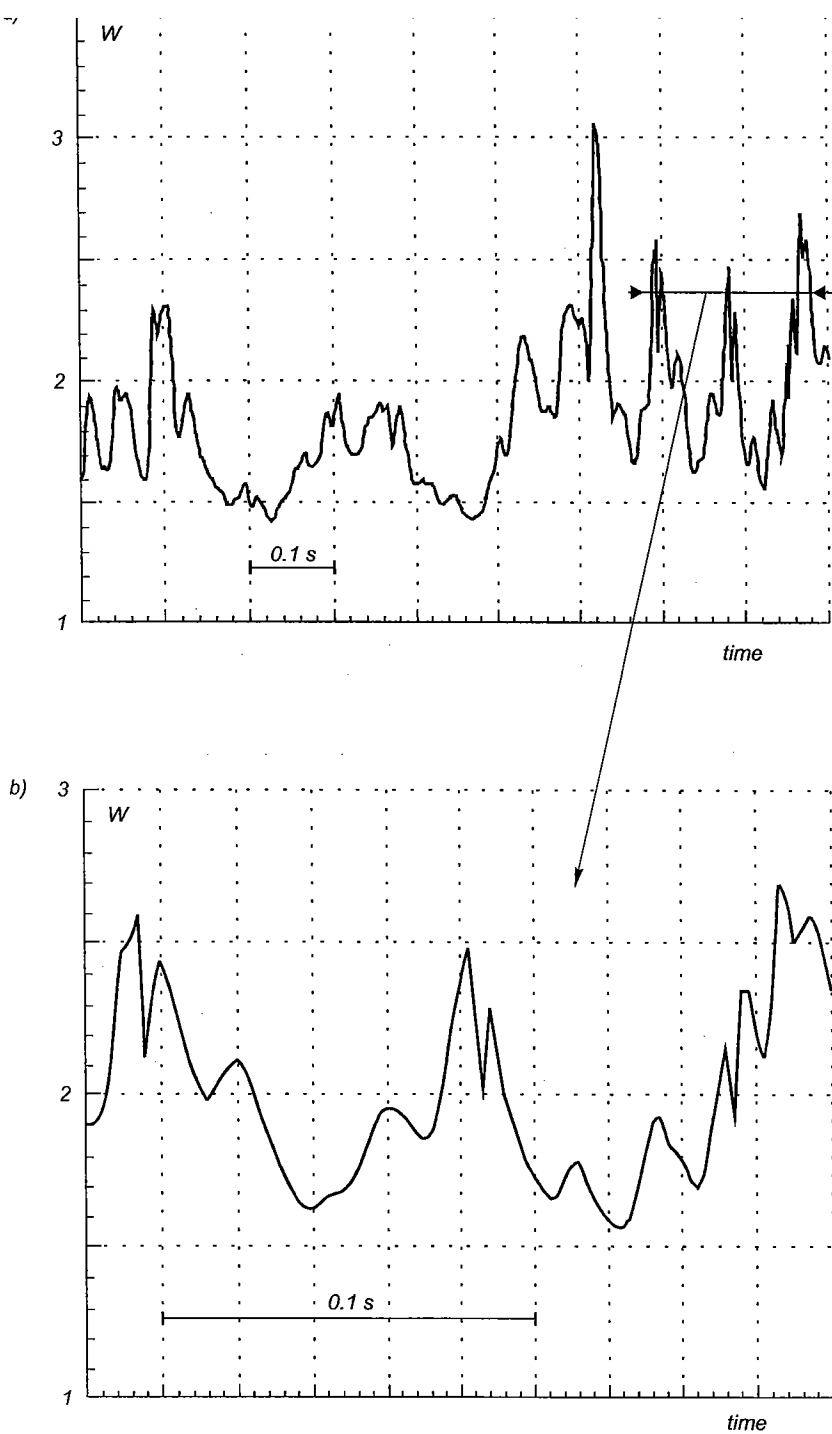


Fig. 4. W fluctuations for $V_G = 0.021$ m/s, $\varphi = 90^\circ$; (b) – „stretched” part of upper signal (a)

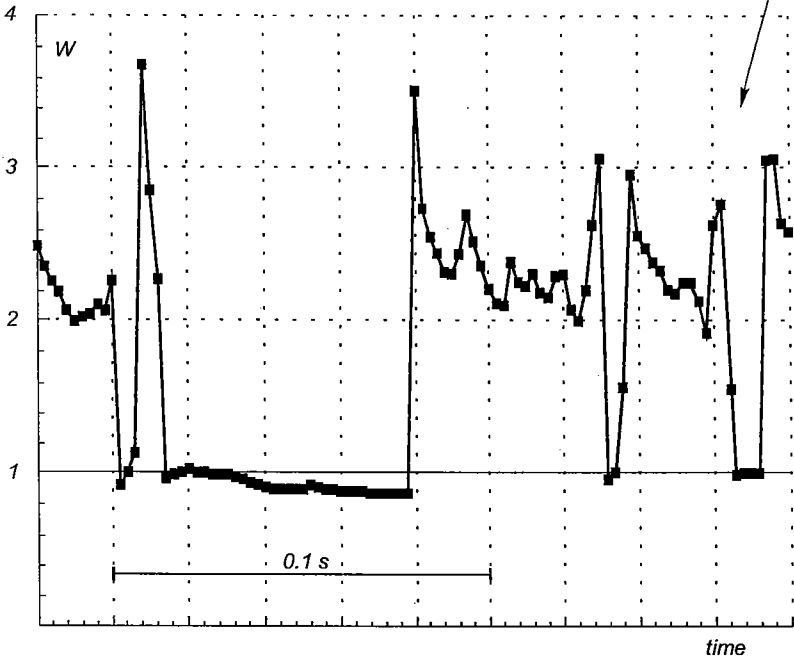
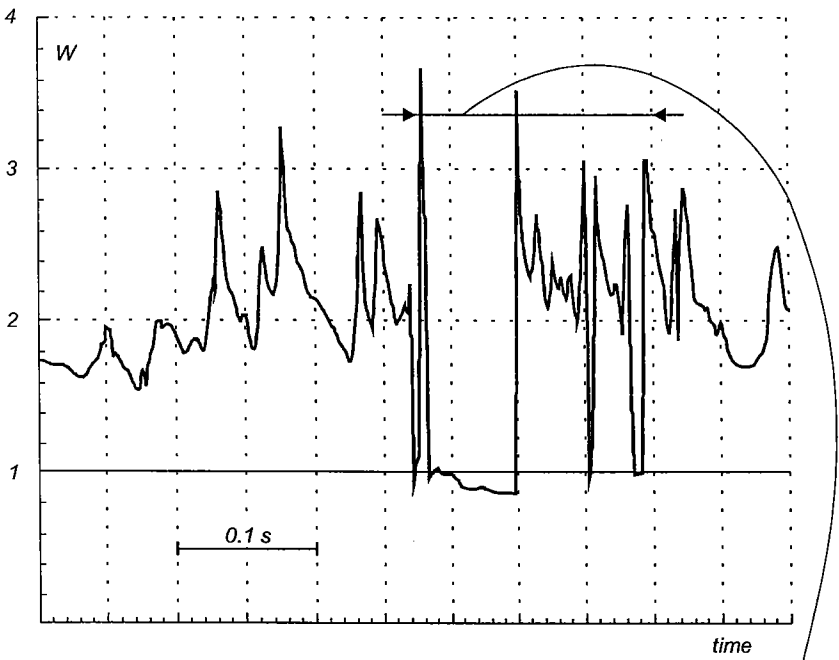


Fig. 5. W fluctuations for $V_G = 0.021\text{ m/s}$, $\varphi = 180^\circ$; (b) – „stretched” part of upper signal (a)

The character of fluctuations strongly depend on sensor position. For angle $\varphi = 90^\circ$ the recorded variations are similar to those described in [10] for wall-column measurements with their main feature being the impulses of large amplitudes (Fig. 4). It is observable that the higher frequency component is embedded in the slower. While the latter is related to the bubble passage frequency the former probably results from the bubbles oscillations. This phenomenon is not observable in the upper part of cylinder. All signals for $\varphi < 90^\circ$ show a relatively slow frequency component and smaller mean value than those for $\varphi > 90^\circ$. The number of impulses observed per time unit is the highest on the bottom part of cylinder – in the region of large bubbles concentration and small velocities. This confirms the explanation of the phenomenon as a result of bubbles oscillations rather than their upward movement. Another important feature typical for $\varphi > 90^\circ$ appear due to the bubbles approaching the wall. The „attached” gas bubble causes the rapid decrease of heat transfer and thus W becomes smaller than one (Fig. 5). The typical time of bubble attachment varies from zero up to 0.05 s and further growth of heat transfer is very fast – W jumps to 2–3 in 0.002 s. This is probably result of rapid interface distortion coupled with the liquid movement in the sensor vicinity.

The autocorrelation functions (ACF) of W are plotted in Fig. 6 and 7. The main discrepancy of the ACF consists in the slope of the curves for particular φ and flow regimes. For the bubble flow (Fig. 6) the time microscale strongly depends on φ with the largest value for $\varphi = 30\text{--}60^\circ$. This tendency decreases with gas superficial velocity V_G . For all flow patterns the microscales for $\varphi = 180^\circ$ are the smallest and close to each other. This is a direct effect of the impulses appearing in the signals.

The estimates of power spectral density functions (PSD) of the raw E signals are illustrated in Fig. 8–13. Since these signals were not processed, the ordinate values have no physical meaning and are given to enable comparison of the intensity of the particular frequency bands. Only the PSD obtained for $\varphi = 90^\circ$ (Fig. 10, 11) give clear indication for flow pattern identification. They are similar to those observed in the wall-measurements with their main features being: small power spread up to 10 s^{-1} for the bubble flow (Fig. 10a), distinctive strong peak at low frequency for the transition regime (Fig. 11a) and the higher components embedded in the predominant low one for the churn flow (Fig. 11b). For $\varphi = 0^\circ$ all the spectra are similar to each other and indicate the strong peak at frequency lower than 1 s^{-1} (Fig. 8, 9) probably due to the water circulation in the vicinity of the upper part of the cylinder [11]. For the bottom part of it ($\varphi = 180^\circ$, Fig. 11, 12) PSD are strongly influenced by the impulses appearing in the signals. This influence is exactly the same as that of the random noise with a large variance. For this reason most of the particular peaks observed have probably no physical reality.

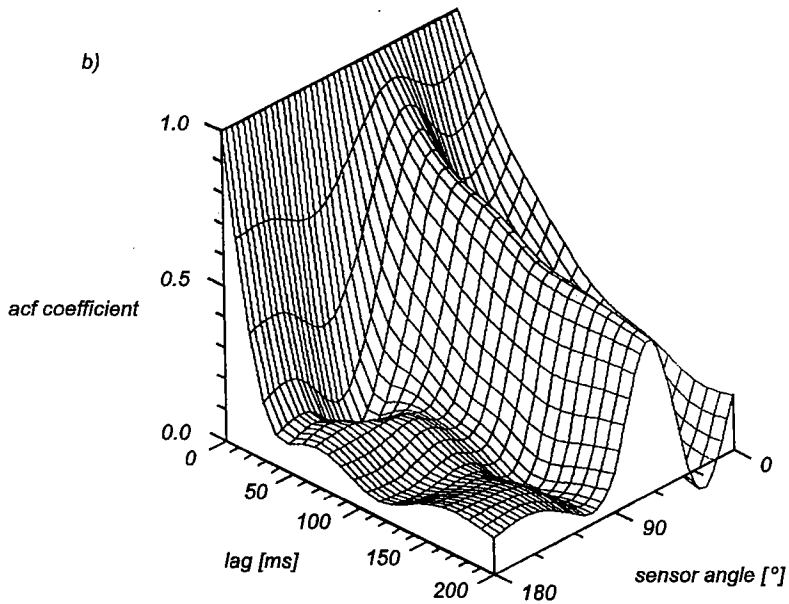
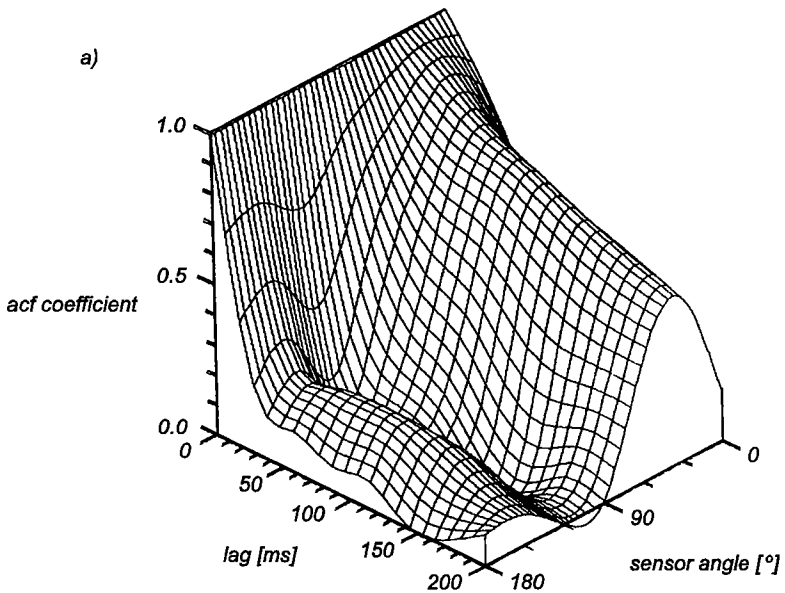


Fig. 6. Autocorrelation function (ACF) vs sensor angle φ for bubble flow regime: a) $V_G = 0.021$ m/s, b) $V_G = 0.042$ m/s

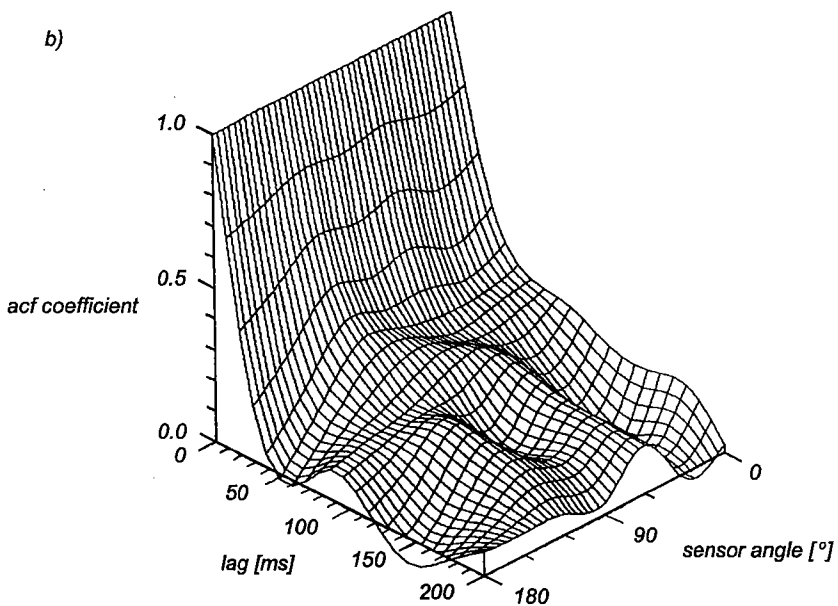
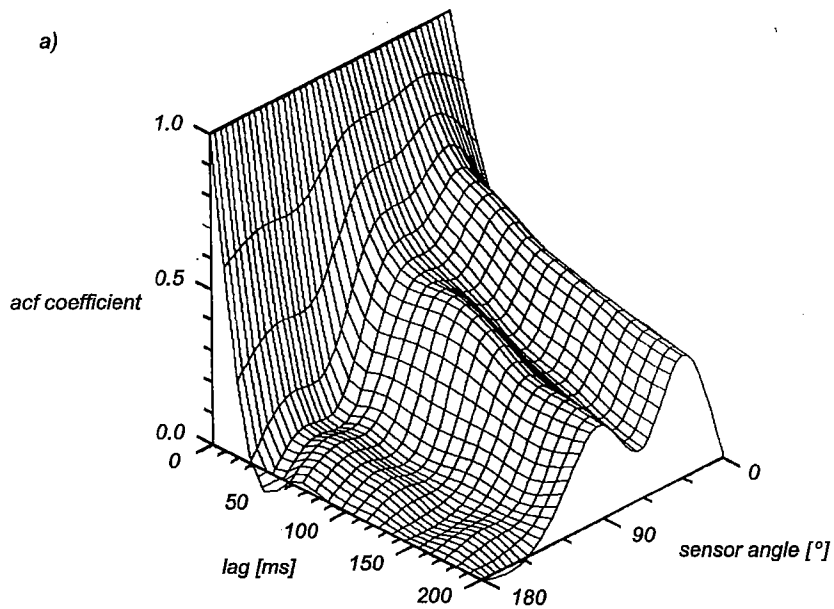


Fig. 7. Autocorrelation function (ACF) vs sensor angle φ for: a) $V_G = 0.063$ m/s, transition regime, b) $V_G = 0.158$ m/s, churn flow regime

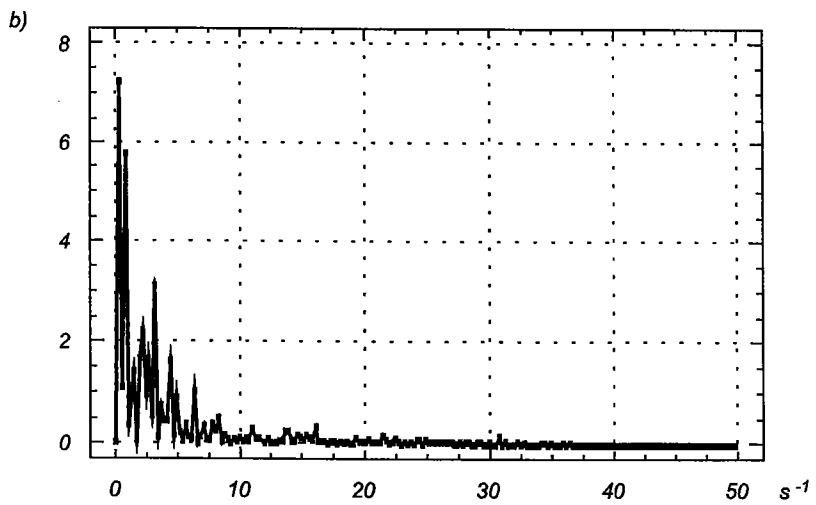
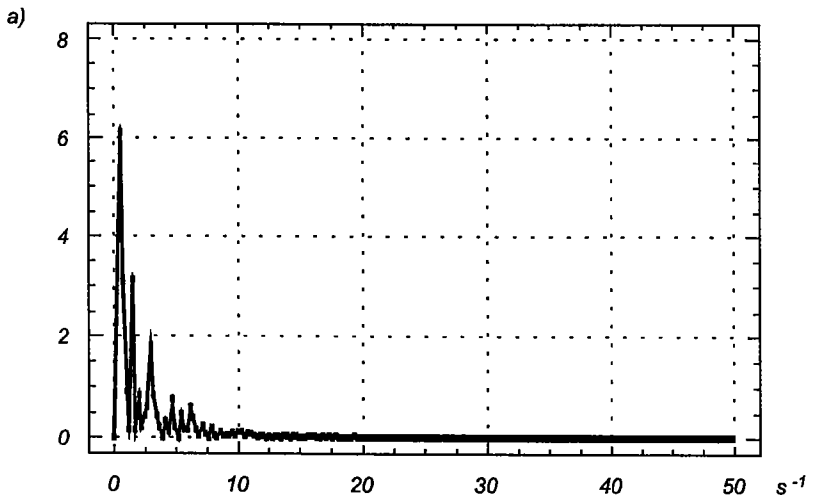


Fig. 8. Power spectral density function (PSD) of E signals for $\varphi = 0^\circ$ and: a) $V_G = 0.021$ m/s,
b) $V_G = 0.042$ m/s

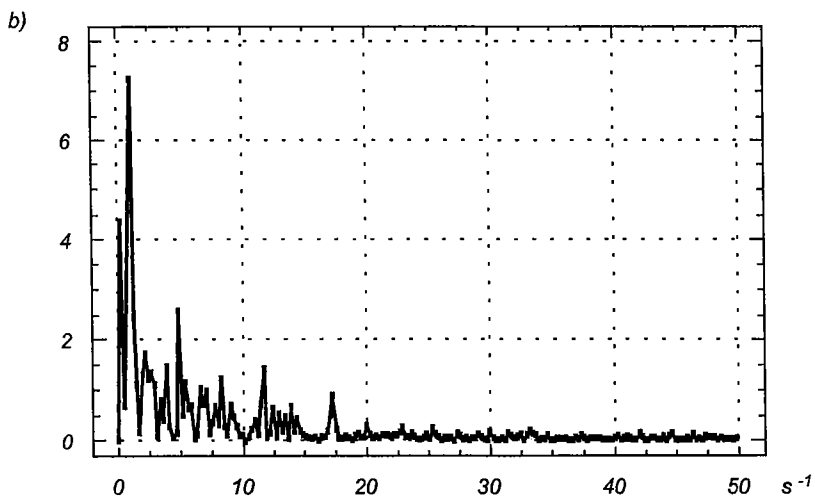
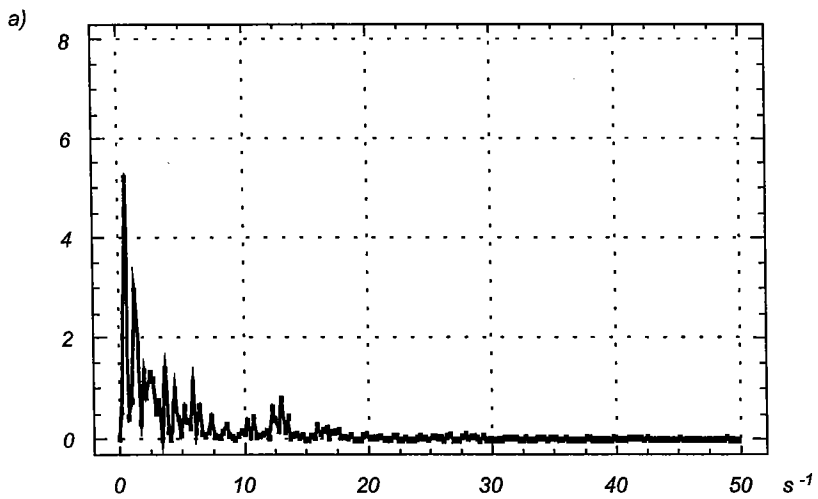


Fig. 9. Power spectral density function (PSD) of E signals for $\varphi = 0^\circ$ and: a) $V_G = 0.063$ m/s,
b) $V_G = 0.158$ m/s

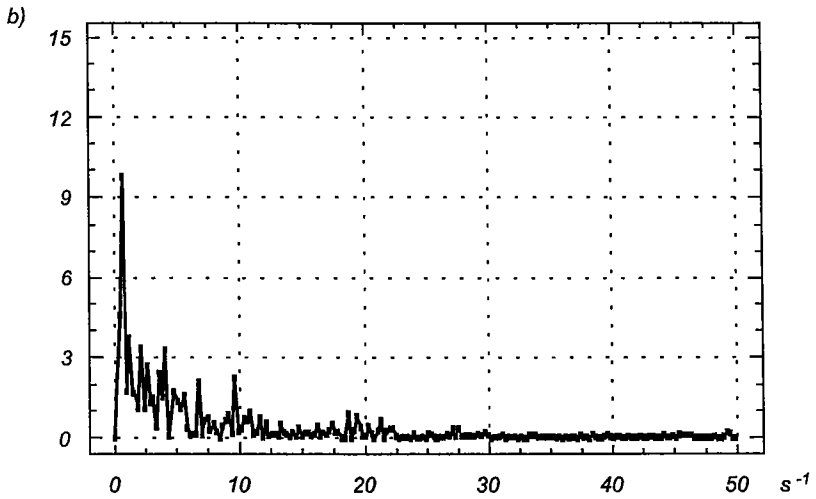
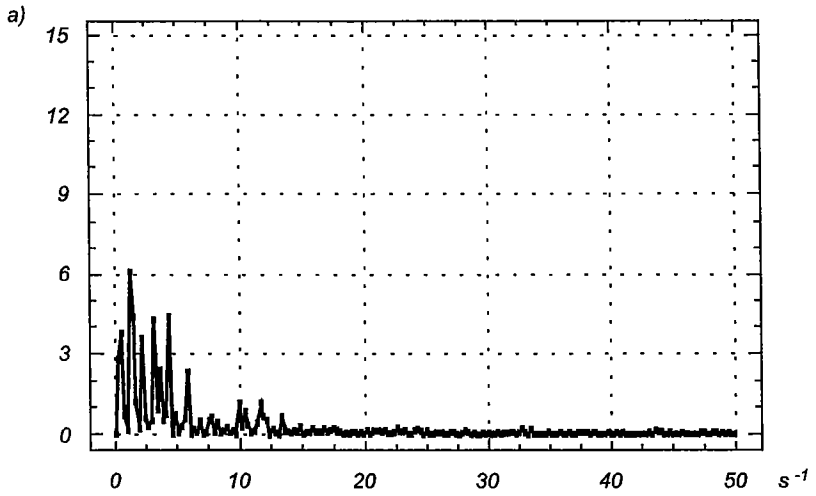


Fig. 10. Power spectral density function (PSD) of E signals for $\varphi = 90^\circ$ and: a) $V_G = 0.021$ m/s, b) $V_G = 0.042$ m/s

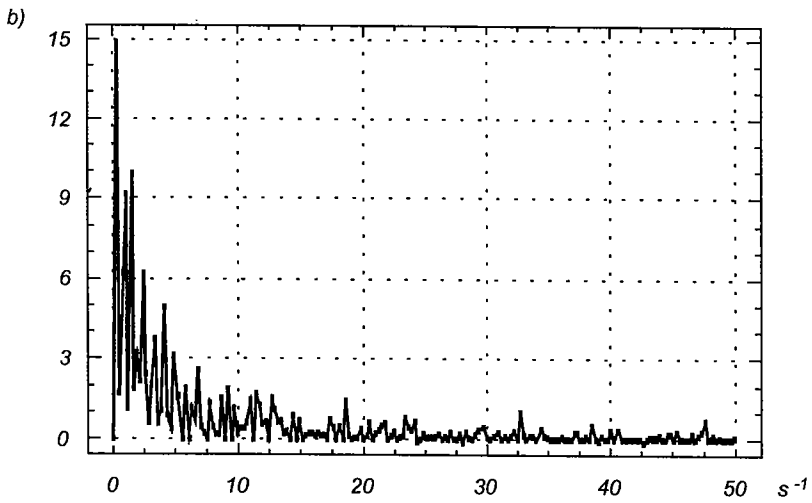
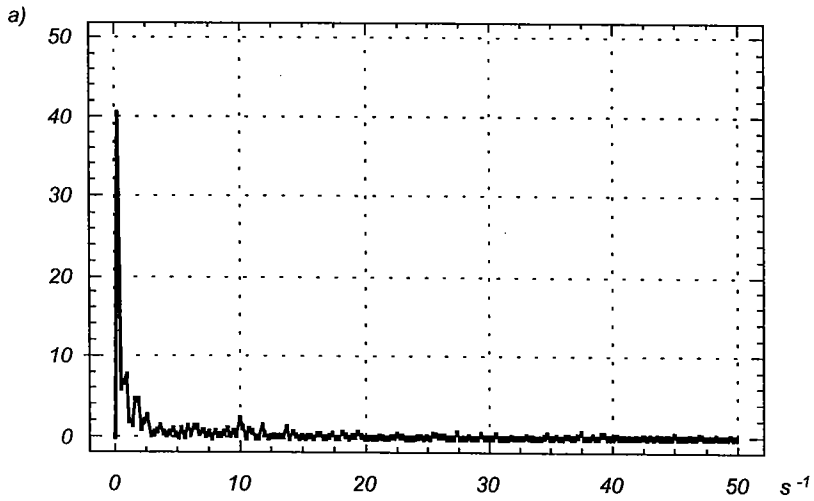


Fig. 11. Power spectral density function (PSD) of E signals for $\varphi = 90^\circ$ and: a) $V_G = 0.063$ m/s,
b) $V_G = 0.158$ m/s

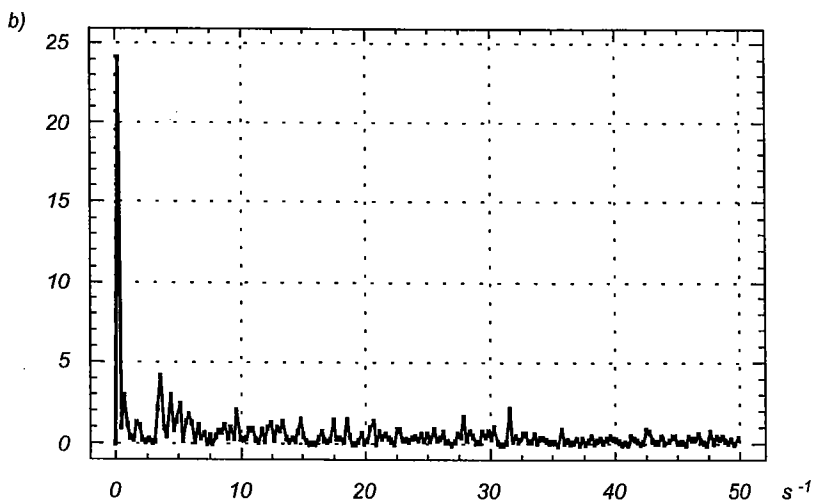
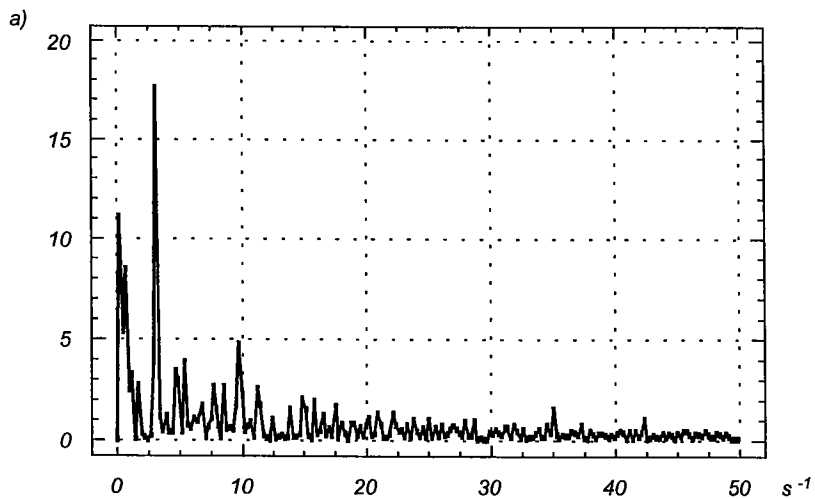


Fig. 12. Power spectral density function (PSD) of E signals for $\varphi = 180^\circ$ and: a) $V_G = 0.021$ m/s,
b) $V_G = 0.042$ m/s

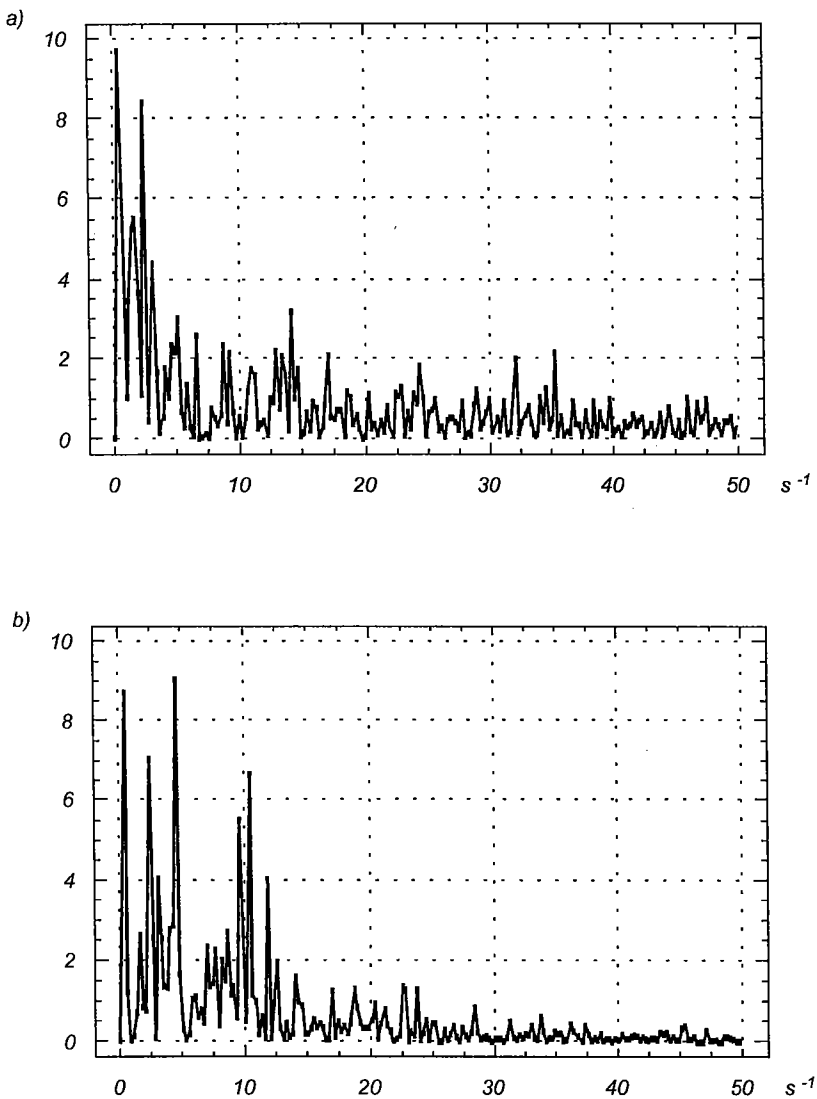


Fig. 13. Power spectral density function (PSD) of E signals for $\varphi = 180^\circ$ and: a) $V_G = 0.063$ m/s, b) $V_G = 0.158$ m/s

It should be noted that also in the churn flow regime the dominant contribution to the flow fluctuations occurs at approx. 1 s^{-1} and also that the fluctuation components above 20 s^{-1} are almost negligible. The latter fact is in some contradiction with the observed signals character for $\varphi = 180^\circ$ (Fig. 5). Thus, selection of the sampling rate according to the above estimation (the Nyquist frequency equal to 20 s^{-1}) may lead to the significant losses of the information about fluctuations nature.

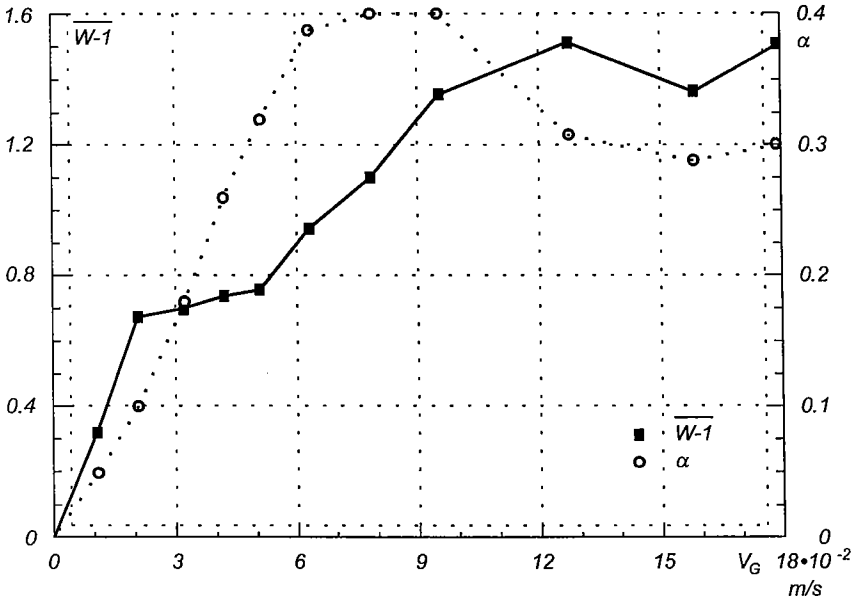


Fig. 14. Void fraction α and averaged $\overline{W-1}$ plotted vs gas superficial velocity V_G for $\varphi = 90^\circ$

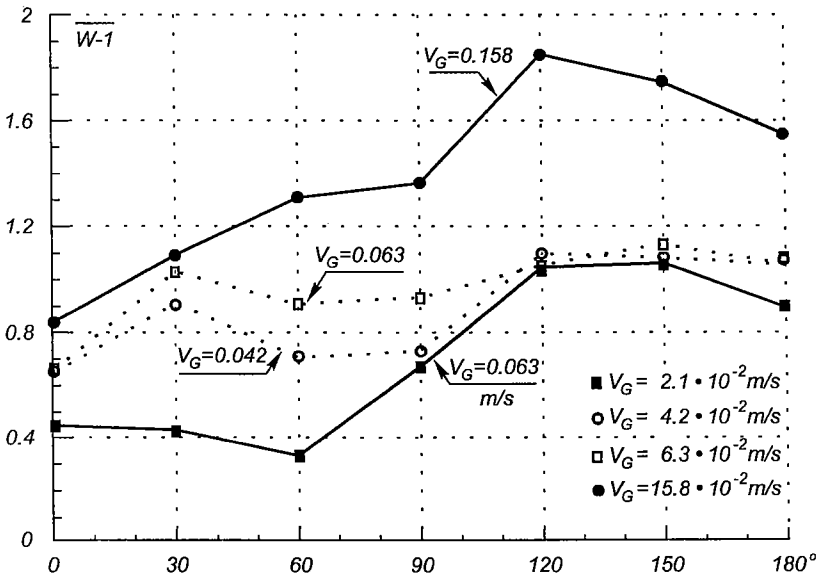


Fig. 15. Averaged value $\overline{W-1}$ plotted vs sensor angle φ for gas superficial velocity $V_G = 0.021, 0.042, 0.063$ and 0.158 m/s

in Fig. 14 the mean value of $W - 1$ and void fraction α are plotted against the gas superficial velocity V_G . The distinct increment of W value occurs at the bubble and transition regimes, while it remains constant after the churn flow boundary is approached. The further increment of V_G and thus the growth of mechanical energy input causes no changes of W . This fact is in contradiction with the theories predicting the direct relationship between the heat transfer and the energy dissipation rate in the two-phase flow. Contrary to the heat transfer from „large” elements ([2, 5]), the major increment of W occurs not only at the bubble flow but also at the transition regime.

The dependence of W on φ is shown in Fig. 15. For all flow structures W is higher on the bottom side of the cylinder. It seems that the high intensity of heat transfer in this region results from large impulse frequency which is not correlated with bubble velocity. Moreover, the bubble attachment to the heated element does not decrease significantly transport phenomena – it probably led to shifting the maximum value of W from $\varphi = 180^\circ$ to $\varphi = 120\text{--}150^\circ$.

REFERENCES

- [1] Stiff A., Weinspach P.M.: Heat transfer in stirred and non-stirred gas-liquid reactors. *Ger. Chem. Eng.* 1978, Vol. 1, p. 150.
- [2] Nishikawa M., Kayo H. and Hashimoto K.: Heat transfer in aerated tower filled with non-Newtonian liquid. *Ind. Eng. Chem. Prog. Des. Dev.* 1977, Vol. 16, p. 133.
- [3] Kast W.: Untersuchungen zum Wärmeübergang in Blasensäulen. *Chem. Ing. Tech.* 1963, Vol. 35, p. 785.
- [4] Calderbank P.H.: Gas absorption from bubbles. *The Chem. Engr.* 1967, Vol. 45, BE209.
- [5] Decrier W.D.: On the mechanism of heat transfer in bubble column reactors. *Chem Eng. Sci.* 1980, Vol. 35, p. 1341.
- [6] Hewitt G.F.: Measurement of two phase flow parameters. Academic Press, London 1978.
- [7] Crawford T.J., Weinberger C.B., Weisman J.: Two-phase flow patterns and void fractions in downward flow. *Int. J. Multiphase Flow.* 1985, Vol. 11, No. 6, p. 761.
- [8] Davis M.R. and Funtamasan B.: Large scale structures in gas-liquid mixture flow. *Int. J. Multiphase Flow.* 1984, Vol. 10, p. 663.
- [9] Ostrowski K.: Bubble flow stability in vertical column. Ph.D. Thesis, Warsaw University of Technology. Warsaw, Poland 1987 (in Polish).
- [10] Ostrowski K.: Heat transfer phenomena in air-water vertical flow. *Proc. of 1st Baltic Heat Transfer Conference*, Elsevier Amsterdam 1992.
- [11] Ostrowski K.: Analysis of small-scale perturbation in air bubbles agitated water. *1st*

- [12] Ostrowski K.: Cooling of small thermal element in air-water flow. *8th Symposium on Heat and Mass Transfer. Białowieża, September 1992.*

POMIARY ZABURZEŃ ZDYSPERSOWANEGO PRZEPIYU DWUFAZOWEGO ZE SZCZEGÓLNYM UWZGLĘDNIENIEM PROCESÓW TRANSPORTU CIEPŁA

Streszczenie

W pracy przedstawiono wyniki pomiarów fluktuacji strumienia ciepła na powierzchni cylindra zamocowanego poziomo w pionowej kolumnie. Badano przepływ powietrza przez słup wody przy pęcherzowej, przejściowej i pienisto-turbulentnej strukturze przepływu. W celu określenia oddziaływań różnoskalowych zaburzeń cieczy na powierzchnię cylindra użyto stałotemperaturowego anemometru z sondą powierzchniową, której czujnikiem była podgrzewana warstwa niklu o wymiarach $0,2 \times 0,75$ mm. Przeprowadzono statystyczną analizę zarejestrowanych sygnałów i niektóre z otrzymanych parametrów przedstawiono w funkcji pozornej prędkości gazu, jego udziału objętościowego oraz położenia czujnika. Wyniki wskazują, iż intensyfikacja wymiany ciepła w badanym procesie zależy w pierwszej kolejności od małych, losowych, lecz anizotropowych zaburzeń pola prędkości w fazie ciekłej.

ИЗМЕРЕНИЯ ПЕРТУРБАЦИИ ДИСПЕРСНОГО ДВУХФАЗНОГО ПОТОКА С ОСОБЫМ УЧЕТОМ ПРОЦЕССОВ ТЕПЛОПЕРЕДАЧИ

Краткое содержание

В работе представлены результаты измерения флуктуации потока тепла на поверхности цилиндра горизонтально закрепленного в вертикальной колонне. Исследовалось течение воздуха через водяной столб при пузырьчатых, переходных и пенисто-турбулентных режимах течения. Чтобы определить воздействие пертурбаций жидкости в разной степени на поверхность цилиндра использован постояннотемпературный анемометр с поверхностным зондом, оптиметром которого был термический элемент размером в $0,2 \times 0,75$ мм. Проведен статистический анализ зарегистрированных сигналов и некоторые из полученных параметров представлены в функции приведенной кажущейся скорости газа, истинного объемного газосодержания и положения оптиметра. Результаты показывают, что главной причиной интенсификации теплообмена являются прежде всего мелкие, случайные, но анизотропные пертурбации поля скорости в жидкой фазе.